Control of gas pipeline leakage detection based on hybrid inline fiber interferometer

Nada F. Noori[1,2], Tahreer S. Mansour[1]

[1]Department of Industrial and Engineering Applications, Institute of Laser for Post Graduate Studies, University of Baghdad, Baghdad, Iraq
[2]Electrical Designs Unit, Department of MEP Designs and Services, National Center for Engineering Consultancy, Baghdad, Iraq

Article Info

ABSTRACT

Hybrid inline fiber interferometers gained attention recently especially in the building control and detection fields due to their hybrid multi-path interferences, multi-parameter measurements, high sensitivity, and high precision. This work used etched multimode fiber (MMF) to introduce a novel medical gas pipeline leakage detector based on hybrid Fabry-Perot/Mach-Zehnder inline fiber interferometer (FP-MZI). The hybrid FP-MZI of this work consisted of two cascaded identical fiber Bragg gratings (FBGs) spliced to coreless fiber sandwiching the MMF. Four samples of different MMF lengths and sizes were used as sensing heads in the detection measurements. Self-imaging and phase-equations of the proposed interferometer were solved analytically to select the required length; then COMSOL software was used to ensure the occurrence of the required interference along the proposed interferometer at the designed wavelength. Two medical gas sources; air compressor and high-pressure gas cylinder, attached to two pipelines of size 15×0.7, and 12×0.6 mm was used to provide the required pressure. Gas leak was introduced to the pipes manually through controlled valves and measured using the proposed hybrid FP-MZI. Both constant and variable gas flowrates was investigated with variable gas pressures. The obtained sensitivity was ranged from 0.17-20.9 pm/bar for all of the investigated cases.

Corresponding Author:

Nada F. Noori
Department of Industrial and Engineering Applications, Institute of Laser for Post Graduate Studies
University of Baghdad
Baghdad, Iraq
Email: nada.fares1101a@ilps.uobaghdad.edu.iq

1. INTRODUCTION

Pipelines are among the most important sections in the world's material and energy transport infrastructures. Many types of pipeline transport systems are used in the world like water pipelines, and sewage pipelines oil pipelines [1]. Since the use of pipeline infrastructures in the world is increasing and aging, the reliable and safe operation of pipelines is highly required too. Because of the intrinsic advantages of optical fibers such as small size, lightweight, immunity to electromagnetic interference, and flexibility [2]; optical fibers played an important role in the implementation of a rigid and accurate pipeline leakage detection system which is considered as one of the main issues of the pipeline condition monitoring especially for petroleum and natural gas pipelines due to their risks and high expenses [2]–[6].

Smart buildings, monitoring, and management systems played an important role in the efficient control of the building services like electrical energy consumption [7]–[9], and security [10]. Therefore; the necessity to build a low cost and efficient monitoring system increased to cover the requirements of smart

buildings especially in hospitals [11]. Hospitals are principal buildings that contain many service infrastructures and the lives of patients depend on the reliability of these infrastructures. Medical gases like oxygen, and nitrogen are considered as crucial infrastructure, and any leak in these pipelines will either affect the amount of required air for critical patients or increase the risk of flames and explosions. In addition, the leakage from tanks of these gases may be very dangerous too [12].

The optical inline fiber interferometers are briefly identified by the interference of optical light waves inside a specially modified structures of optical fibers to undergo optical interference [13], [14]. In addition to the sharp and tunable optical filters [15], [16] inline fiber interferometers showed wide success in fine and accurate detection and sensing applications of temperature, pressure, vibration and so on due to the advantages of vernier effect and fine modal interference that occurs inside [17]–[19] etching, tapering, or clad reduction to the optical fibers can largely alter the mode propagation along the optical fibers as long as it alters the effective refractive index of the propagating wavelength and thus new interference modes can be obtained inside the etched fiber (i.e., excitation to the higher-order modes). The change of effective index of the etched fiber is usually characterized or examined by the final obtained central wavelength, maximum power, and spectral width [20], [21]. Hybrid inline fiber interferometers are simply defined as a mixture of two or more types of fiber interferometers and the hybrid Mach-Zehnder/Fabry-Perot inline fiber interferometer is a simple, easily implemented with good accuracy one [22], [23]. Hybrid inline fiber interferometers gained attention in recent years due to their good coherence properties, hybrid multi-path interference, high precision in sensing applications, ease of implementation, low cost, high integration, dual-parameter measurement capability and low cross sensitivity [24], [25].

This work introduces a novel inline fiber interferometer that has hybrid interference behavior among Mach-Zehnder interferometer, Fabry-Perot interferometer, and modal interferometer to work as a medical gas pipe leakage detector. The interferometer of this work is implemented using two semi-identical fiber Bragg gratings (FBGs) and two coreless fibers NC that are sandwiching an etched multimode fiber multimode fiber (MMF). The proposed interferometer was tested to detect the gas leak from two medical gas pipes (12×0.6 and 15×0.7 mm) and interlock for two different cases. The first one, the medical gas was provided by a medical cylinder of 10 bar and 10-liter size; while the second case stood for an air compressor that pumps 4 bar and fixed flow rate of 69.7 ml/min. The interferometer sensitivity to the gas leak was characterized by wavelength shift, power change, and spectral width change; sensitivity 0.17-20.9 pm/bar range was obtained from the different investigated cases by this work proposed detector.

2.   THEORY

The interference of any optical fiber interferometer is generally determined using the intensity of interfering waves and phase difference between them; hence for two interfering waves, the intensity of the resulted interference wave can be expressed as shown in (1) [26], [27].

$$I_{tot} = I_1 + I_2 + 2\sqrt{I_1 I_2} \cos \emptyset \qquad (1)$$

Where I_{tot} refers to the intensity of total interference wave, I_1, I_2 are the intensity of the first and second interfering waves, and ϕ is the phase difference between the interfering waves that can be calculated using (2) [13], [14].

$$\emptyset = \frac{2\pi\, n_{eff} L}{\lambda} \qquad (2)$$

Where; n_{eff}: is the effective refractive index of the propagating mode along the optical fiber at the interference region, L is the optical path length of the interfering wave along the optical fiber, and λ is the operational wavelength [28].

The structure of the hybrid inline fiber interferometer proposed in this work consists of an etched MMF of 50/125 μm core to cladding size, 1.476 effective refractive index, two coreless fibers (Thorlabs-FG125LA) with 1.444 effective index value at 1550 nm, and clad size of 125 μm, spliced to the both ends of MMF, and two FBGs of 1546.7 nm central wavelength, 10 mm grating length, reflectivity greater than 90% (i.e., 95 and 94% for input and output respectively), and bandwidth of 0.2 nm; these components were spliced to sandwich the coreless-MMF fibers as shown in Figure 1. Before going along with the analysis behavior of the proposed inline interferometer of this work; we need to keep in mind that the main structure of any optical fiber Mach- Zehnder interferometer is basically raised from the interference of the recombination of at least two or more arms of coherent light (i.e., the best case is to be obtained from the same optical source) [13], [27], [29]. In contrast; the Fabry-Perot interferometers are generally obtained from the interference of forward and backward waves that are reflecting between two reflective surfaces [13], [22], [25]. The analyzation of the

behavior of the proposed interferometer can be carried out according to two hypothesises. The first one is the propagating light out of the first FBG entering the first coreless fiber will be dispersed into a several parallel waves to act like Mach-Zehnder interferometer arms; then they recombined again in the second single-mode fiber where the first type of interference is obtained. The purpose of the multimode fiber here is to maintain the guiding for the produced arms.

The second hypothesis is when the first recombined wave hits the second FBG; a part of it will be reflected to the second coreless fiber and undergo the same expansion and recombination in the first hypothesis of the Mach-Zehnder interferometer until it reaches to the first FBG again. Both FBGs have the near same reflectivity and hence Fabry-Perot like behavior is obtained from the interference of forward and backward reflected waves between FBGs. Therefore, according to the explained hypothesises; the proposed inline fiber interferometer has hybrid interference behavior between Mach-Zehnder and Fabry-Perot interferometers. Thus, the total intensity out of the interferometer should be calculated by taking into consideration the hybrid interference of the four proposed waves; the forward and backward waves of Fabry-Perot and the Mach-Zehnder recombined waves using (3) [30].

$$I_{tot} = I_{1-MZI} + I_{2-MZI} + I_{FW-FP} + I_{BW-FP} + 2\sqrt{I_{1-MZI}I_{2-MZI}}\cos\frac{2\pi\Delta n_{eff-mzi}L_{mzi}}{\lambda}$$
$$+2\sqrt{I_{FW-FP}I_{BW-FP}}\cos\frac{4\pi\Delta n_{eff-FP}L_{FP}}{\lambda} \tag{3}$$
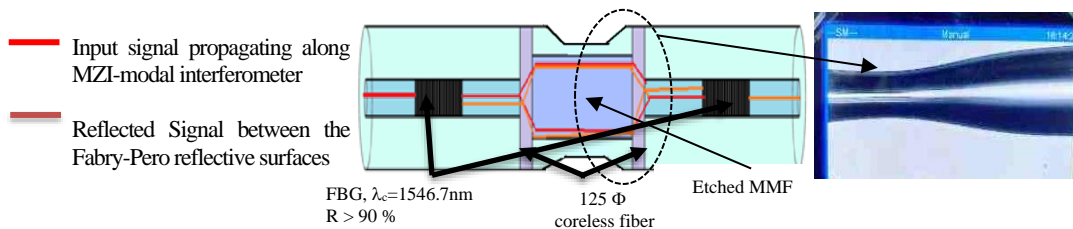

Figure 1. Schematic diagram of the structure of the proposed hybrid inline fiber interferometer

Since the refractive index is a function to the propagating wavelength along any optical fiber [31]; then according to (2) the fiber length will be the key parameter of any inline fiber interferometer because the fiber length decides the optical length of each interfering wave along the interferometer [32]. The multimode interference analysis is mostly the best comprehensive theoretical tool to describe self-imaging phenomena in cascaded multimode fiber waveguides. Therefore, this work made use of the self-imaging relation shown in (4) that links between the required waveguide length, clad-diameter size, wavelength and effective refractive index to decide the required length of the multimode fiber and coreless fiber [33]–[35].

$$L_{MMF} = \rho \times (\frac{n_{eff}\times D_{cl}^2}{\lambda_0}) \tag{4}$$

Where; L_{MMF}: is the required length for the multimode fiber and coreless fiber that satisfies the self-imaging condition, n_{eff} is the effective index for the operating wavelength λ_0 inside the multimode fiber which is equal to 1.444 and 1.476 for coreless and MMF respectively at 1550 nm propagating wavelength (i.e., Thorlabs datasheet of coreless fiber and corning data sheet of MMF), ρ represent the number of reproduced multimode interference image for the defined length, and D is clad diameter size. For gas pipe leakage detection, the leaked gas (i.e., oxygen and nitrogen medical gases) from a pinhole in the pipe or from the interlocks will force the fiber to vibrate randomly with stressing pressure on the fiber related to its escaping flow rate [4]. It was found previously that gas leakage produces a shift in the multimode interference image, which in turn, produces a spectral shift and a change in intensity [1], [5]. As long as the reduction of the clad size by etching or tapering will cause longer evanescent wave tailing along the optical fiber. Therefore, sensitivity of the fiber will be enhanced in terms of physical parameters such as effective refractive index, and strain. According to the above; in order to build a highly sensitive inline fiber interferometer, this work used hydrofluoric acid HF to etch the sensing area of the inline fiber interferometer which is represented by the multimode region [19], [34]-[36]. The multimode etching process for 10, 20, and 30 min using HF resulted in MMF clad reduction thus new clad sizes were obtained which are 108, 89.7, 69.6 µm as shown in Figure 2. Where Figure 2(a) represents the microscopic image of 10 min. etched MMF sample measured along three sequent points of the etched fiber.

While Figure 2(b) represents the amount of remained MMF clad of 30 min etched MMF measured under the same electronic microscope and for three sequent points too.

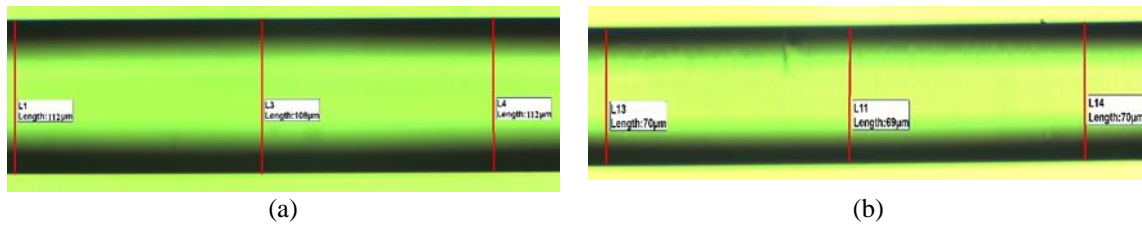(a)   (b)

Figure 2. Microscopic image for the etched MMF segments (a) 10 min etching and (b) 30 min etching

The final design of the required length of the coreless and multimode fibers were done after solving (2) and (4) analytically using MATLAB as shown in Table 1 and Figure 3. The required length of the MMF that satisfies image reproduction along the MMF for one, five and ten times according to the amount of removed clad layer by HF etching is estimated and represented Figure 3(a). While Figure 3(b) shows the estimated developed phase shift along the proposed hybrid interferometer corresponding to the designed fiber lengths.

Table 1. Interferometer designed length according to etching parameters

Etching period (min)	New clad size (µm)	Designed MMF fiber length (cm)
0	125	8.9
10	108	7.2
20	89	4.5
30	69	2.7

(a)   (b)
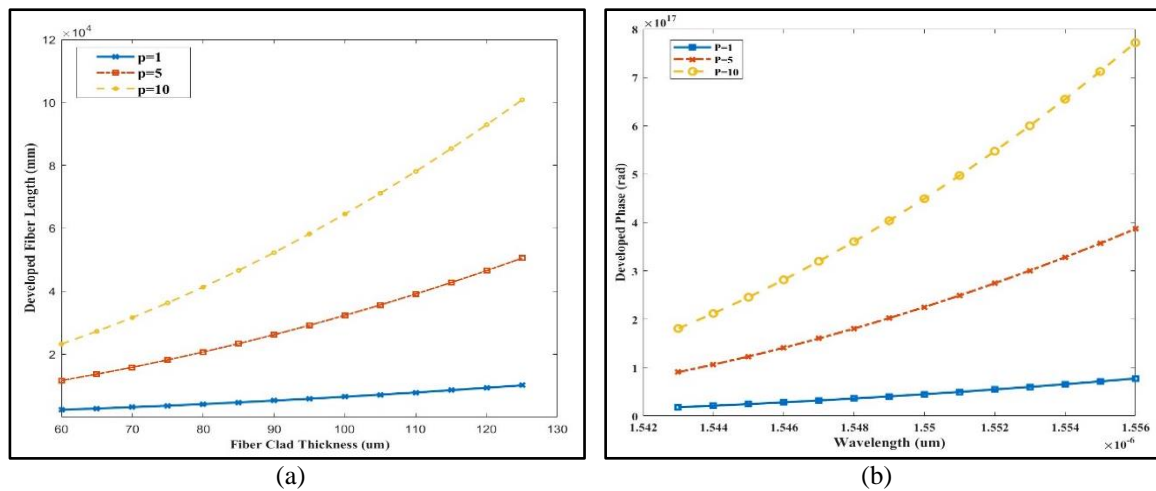
Figure 3. The analytical solution to (2) and (4) represents (a) the required multimode fiber length of the proposed hybrid interferometer and (b) theoretically the developed phase over the proposed hybrid interferometer

The proposed interferometer structure was tested for the interference and its optical paths using COMSOL (5.5) software. Boundary mode analysis under the wave optics physics of COMSOL was used to characterize the propagating modes along with the proposed hybrid Fabry-Perot/Mach-Zehnder (FP-MZI) inline fiber interferometer. Four samples of the interferometer with different multimode clad sizes were simulated and verified by COMSOL. The simulated fiber Bragg grating was of period Λ=0.52988 µm corresponding to central Bragg wavelength λ_B=1546 nm, about 2000 Bragg period were implemented to reach reflectivity greater than 90%, and grating length of 10 mm which are the characteristics of the FBGs that are used in the gas leakage detection system of the experimental part of this work. The simulation results of COMSOL software of the proposed FP-MZI are presented in Figures 4-6, these results showed that the

interference is achieved at the designed central wavelength, and the periodic hybrid interference between the MZI arms waves and the FPI reflected wave as propagating modes is achieved too along the interferometer in the four proposed hybrid interferometer samples.

The inline Mach-Zehnder arms formed at the interface between single and multi-mode fibers is achieved as presented in Figures 4-6(a) by parallel arrays and zigzag arrays met at their interference nodes. Fabry-Perot forward and backward interfering waves were achieved and presented in Figures 4-6(a) too by slight zigzag modes developed according to the phase of reflection within each arm of interference. The proposed interferometer was implemented to operate at laser central wavelength of 1546.7 nm and this operational wavelength was achieved too as shown in Figure 4(b), and (c). Figure 4(b) presents the maximum peak of transmitted and reflected powers out from the proposed hybrid interferometer while Figure 4(c) illustrate the theoretically obtained output power from the proposed hybrid interferometer for unetched MMF which is centered at the designed 1546.7 nm wavelength. Best reproduced interference sample case of the proposed hybrid FP-MZI of this work is shown in Figure 5(a) corresponding to 89.7 µm MMF clad thickness. It shows best periodic hybrid interference and wide transmission band as illustrated in Figure 5(c) which shows highest sensitivity later in the experimental part. Figure 5(c) shows that the highest theoretically obtained power wave centered at the designed wavelength 1546.7 nm. Also it is obvious from simulation results that hybrid interference can results in developing two operational transmission and reflection peaks of the Fabry Perot and as the second peak is generated by the interference of the Mach-Zehnder arms at the etched region as shown in Figure 5(b) and (c) This type of interferometer was recorded as good band pass and notch filter [15], [16], [37]. However highest theoretical output power with sharpest peak was obtained from the 125 µm clad size without etching shown in Figure 4(c) which is also proved in the experimental part in Figure 11. Finally, the theoretically obtained hybrid interference from the 69 µm is presented in Figure 6(a) while the theoretically estimated transmittance and reflectance are shown in Figure 6(b) and the maximum theoretical obtained output power from this interferometer was 20.5 µW centered at 1547 nm as shown in Figure 6(c).
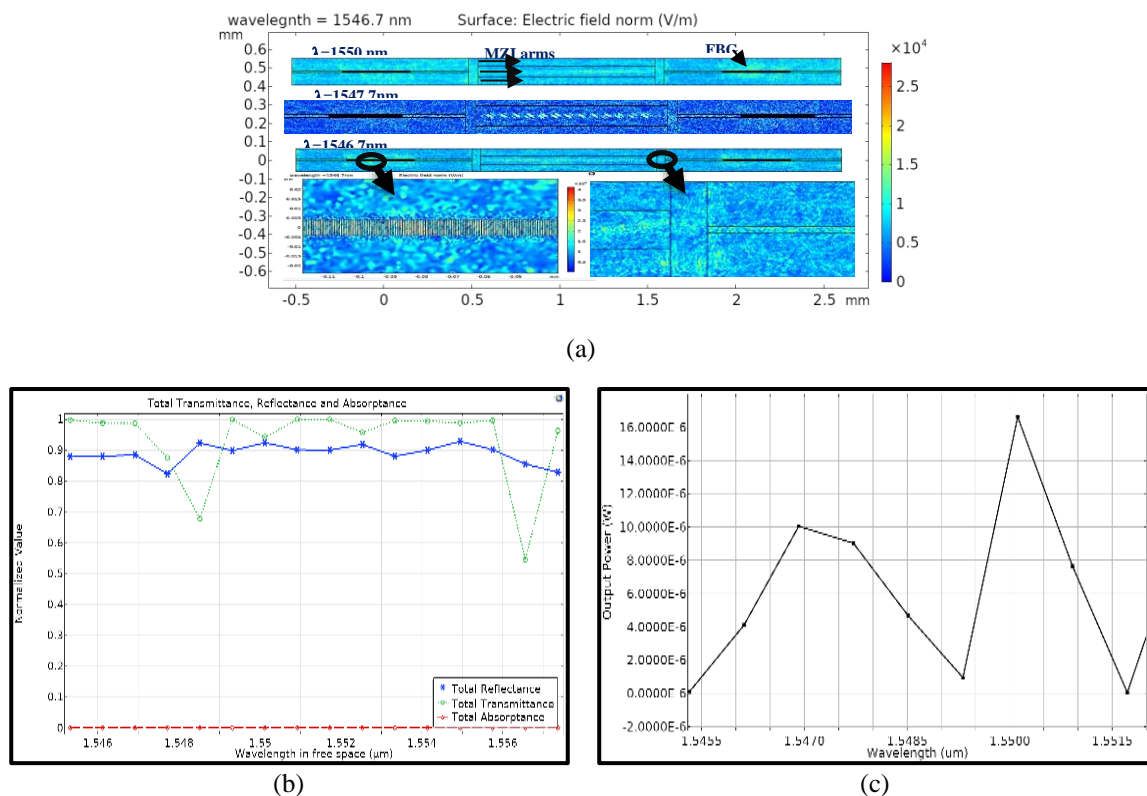

(a)

(b)

(c)

Figure. 4 The theoretical boundary mode analysis of FP-MZI (a) longitudinal modes distribution for FP-MZI of 125 µm MMF sensing head showing the generated Mach-Zehnder arms and the interference between forward, backward waved of the FBGs, (b) obtained total transmittance reflectance and absorptance and (c) theoretical obtained output power from the Interferometer when input source was 1.3mW corresponding to the laser diode power of experimental part
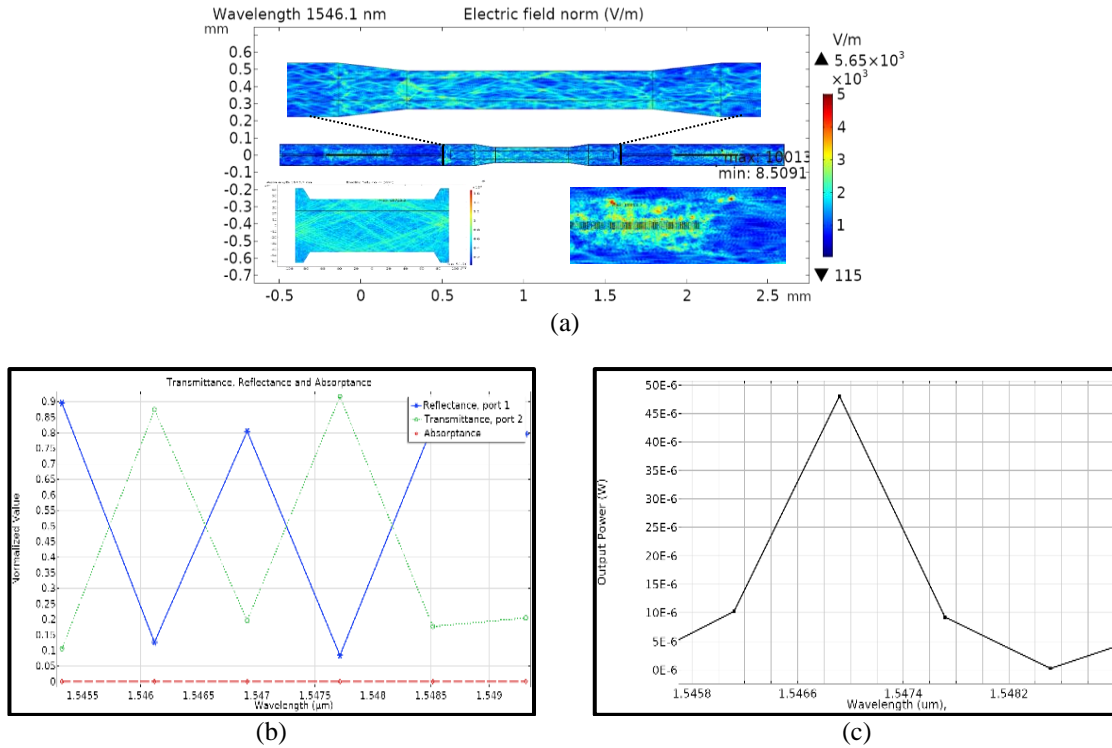
Figure 5. The theoretical boundary mode analysis of FP-MZI (a) longitudinal modes distribution for FP-MZI of 89.7 µm clad MMF sensing head and (b) obtained total transmittance reflectance and absorbance (c) Theoretical obtained output power from the Interferometer when input source was 1.3 mW
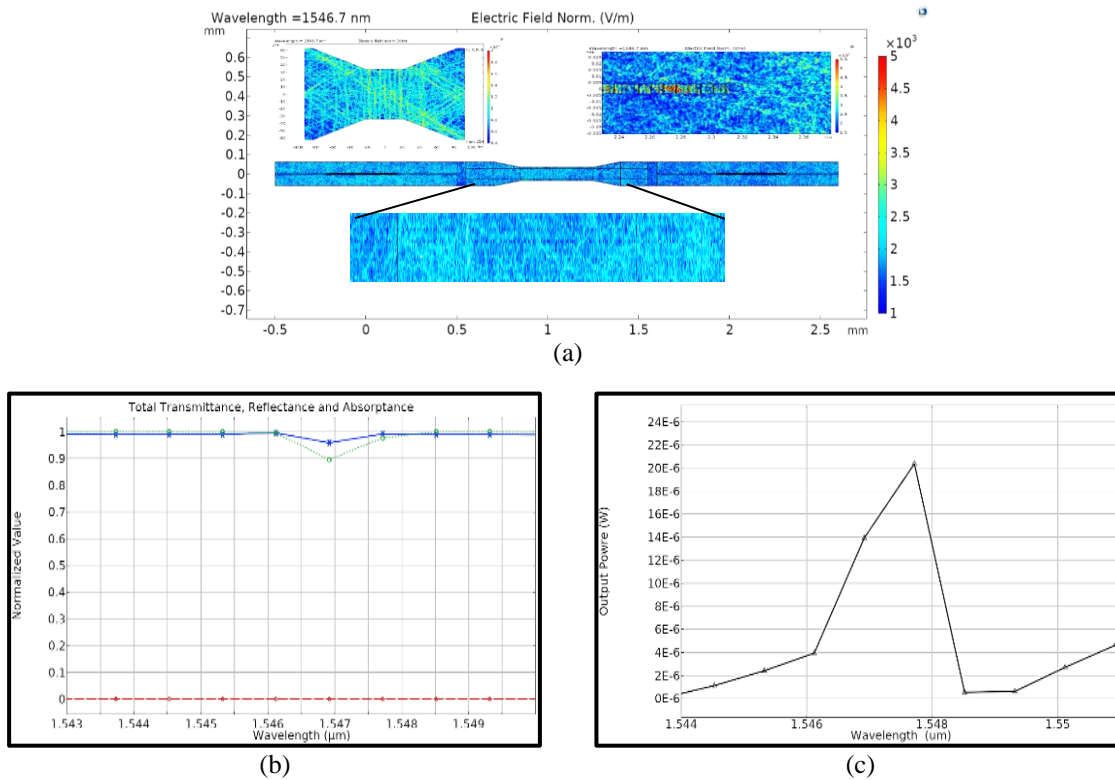

Figure 6. The theoretical boundary mode analysis of FP-MZI (a) longitudinal modes distribution FP-MZI of 69.6 µm clad multimode fiber sensing head, (b) obtained total transmittance reflectance and absorptance and (c) Theoretical obtained output power from the Interferometer when input source was 1.3 mW

3. METHOD AND EXPERIMENTAL PROCEDURES

The experimental procedures in this work were carried out in two steps: the first step was the implementation of the hybrid FP-MZI according to the above theoretical designs; while the second step was applying the hybrid FP-MZI detector to measure the leak from medical gas pipeline systems. The second experimental part was accomplished using two different types of medical gas sources; a compressor, and a high-pressure gas vessel. The proposed hybrid FP-MZI detector was implemented experimentally as shown in Figure 7. Which consists of a laser diode of central wavelength 1546.7 nm, peak power 1.3 mW, 0.2 nm bandwidth. A polarization controller (Thorlabs) was used to maintain perpendicular polarization along and the fiber and to reduce the effect of polarization rotation and polarization mode dispersion along the interferometer. A FBGA interrogator (Bay-spec) was used as a visualizer. Finally, the interferometer structure which was implemented using two identical fiber Bragg gratings. The used FBGs were of 1546.69 nm and 1546.72 nm central Bragg wavelengths, 0.2 nm bandwidth, 10 mm grating length and 0.5288 nm grating period; were connected to two 1 cm equal length coreless termination fibers of 125 µm clad size (FG125LA-Thorlabs), and 1.444 glass refractive index at 1550 nm. Four multimode 50/125 fibers of 8.9, 7.16, 4.5, and 2.7 cm corresponding to these following clad sizes 125, 108, 89.7, and 69.6 µm were spliced at the middle section of the interferometer structure.
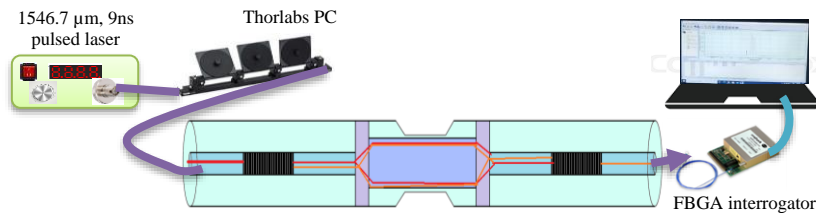

Figure 7. Schematic diagram of experimental FP-MZI detector set-up

According to the British standards of medical pipelines and gases BS-EN 13348; two 1m, Cu-DHP grade Copper medical pipes of 12×0.6 mm and 15×0.7 mm were connected with sealed interlocks to a compressor at one time and medical high-pressure gas cylinder in another time. Again, according to the British standards of medical gas pipelines, the operating pressure must be 7 bar for large pipelines next to the provider (control room) and 4 bar for the smaller pipelines at the end-user side. This work examined only the smaller pipes near the end user to detect the leak. Since the gas pressure and flow rate are the main parameters that can describe the gas leakage from the pipelines [5]. Therefore, the leak was measured for variable pressure and flowrate. The experimental setup for the pipe leak detection experiment is illustrated in Figure 8. Which is consists from the proposed hybrid FP-MZI and the gas pipeline system in addition to the optical source and visualizer. These measurements were carried out in terms of wavelength shift, peak power change, and spectral width. The measurement of a gas pipeline leakage was done using DOT-3AA2015/TC-3AAM154 high-pressure gas vessel, which was carried for variable flowrates and variable pressure as shown in Figure 8(a). In addition; another measurement for variable pressure from the compressor (Linkslauf) at fixed flow rate of 69.7 ml/min were carried out to as shown in Figure 8(b).

Regarding the case of air compressor aided with flow controller knob; gas pressure of 4, 3 to 1 bar was delivered along the pipelines used in this work. In contrast to the case of gas cylinder, both pressure and flowrate were variables, therefore a gas flowmeter (Restek-6000) was used to measure the reference flow value for each examined leaked. The leak was induced in a pipe interlock using a controlling valve with a hole diameter of 1 mm attached to the interferometer and the flow meter end-tip. The relation between each pressure value from the gas cylinder with its corresponding flowrate is stated in Table 2.

Table 2. The measured gas pressure with its corresponding measured flow rate

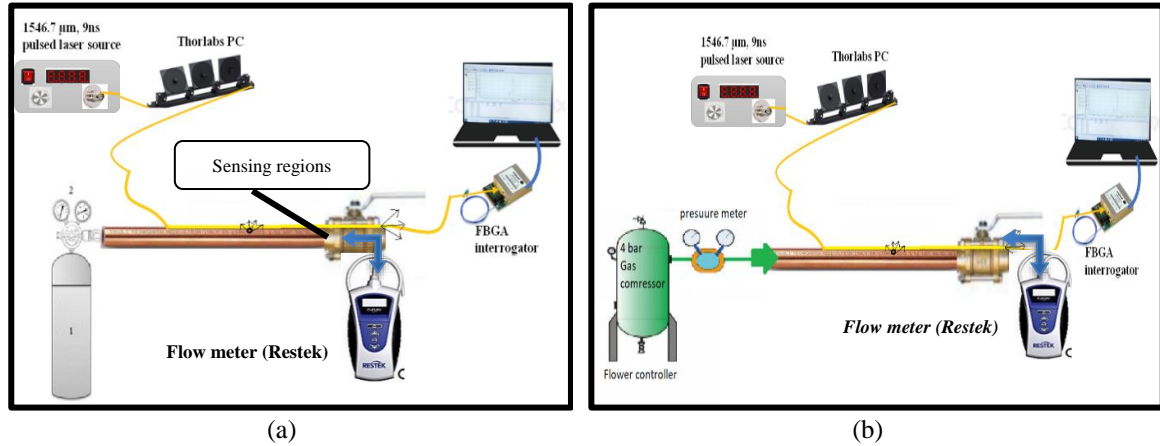| 15×0.7 mm pipe size			12×0.6 mm pipe size		
Pressure (kg/cm2)	Pressure (bar)	Flow rate (ml/min)	Pressure (kg/cm2)	Pressure (mbar)	Flow rate (ml/min)
0	0	0	0	0	0
25	24.5	12	10	0.981	3
50	490	25	25	24.5	7
75	73.5	38	50	49.0	15
100	98.1	53	75	73.5	20
125	123	75	100	98.1	35.3
150	147	95	110	108	42.3

Figure 8. The schematic diagram of the experimental arrangements of the medical gases pipeline leakage detection system, (a) high pressure cylinder with pressure meter used to provide the experiment with medical gases and (b) air compressor with pressure meter and flow controller used to provide the gas

4.   RESULTS AND DISCUSSION

The spectral analysis of the experimental results of the proposed hybrid FP-MZI detector measured with the FBGA interrogator are illustrated for both gas sources; air compressor, and gas cylinder respectively in Figure 9 with its corresponding curve fit of the wavelength shift under the leaked gas pressure. Figure 9(a) shows the experimentally obtained spectra for variable applied gas pressure from air compressor where red shift to central wavelength obtained by increasing the applied gas pressure. In contrast to the case of variable applied gas pressure from gas cylinder presented in Figure 9(b) where the central transmitted wavelength shifts toward shorter wavelengths when the applied gas pressure was increased. The sensitivity of the proposed interferometer was calculated for all of the investigated cases and presented in Table 3. The other obtained relationships between the leaked gas and light parameters of the investigated samples are shown in Figures 10 and 11.
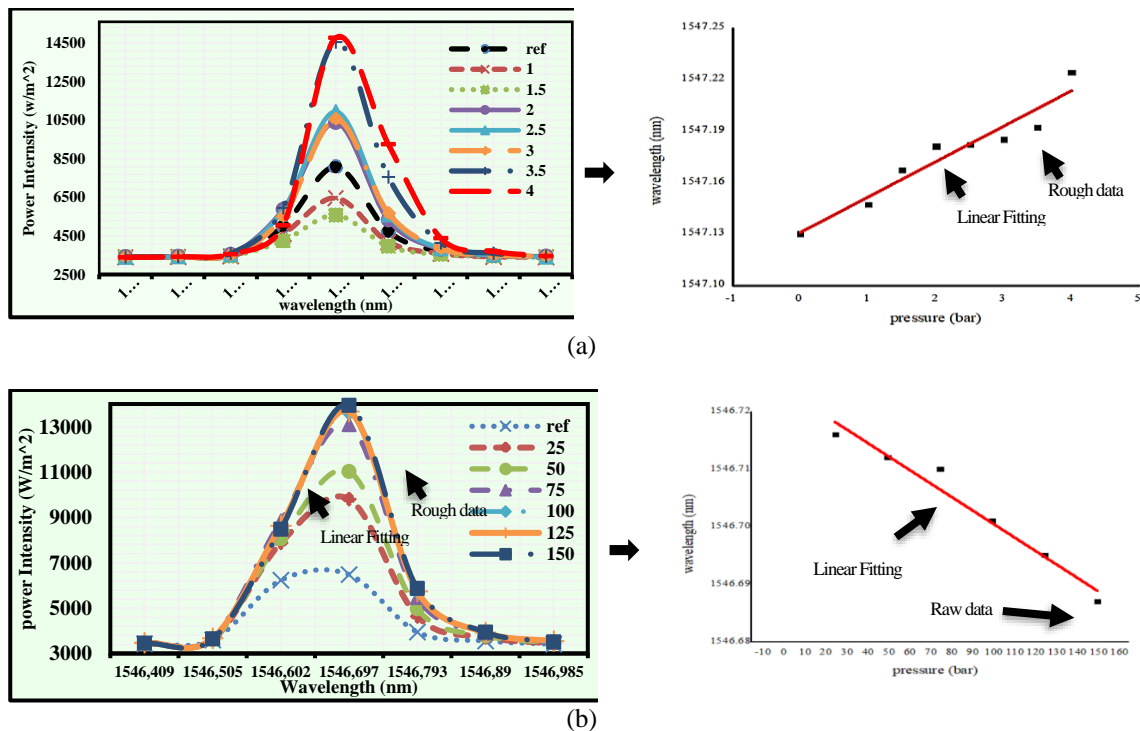

Figure 9. The measured spectrum out from hybrid FP-MZI with its corresponding calculated sensitivity (a) air compressor source and (b) gas cylinder source

Table 3. The obtained sensitivity form all of the investigated cases

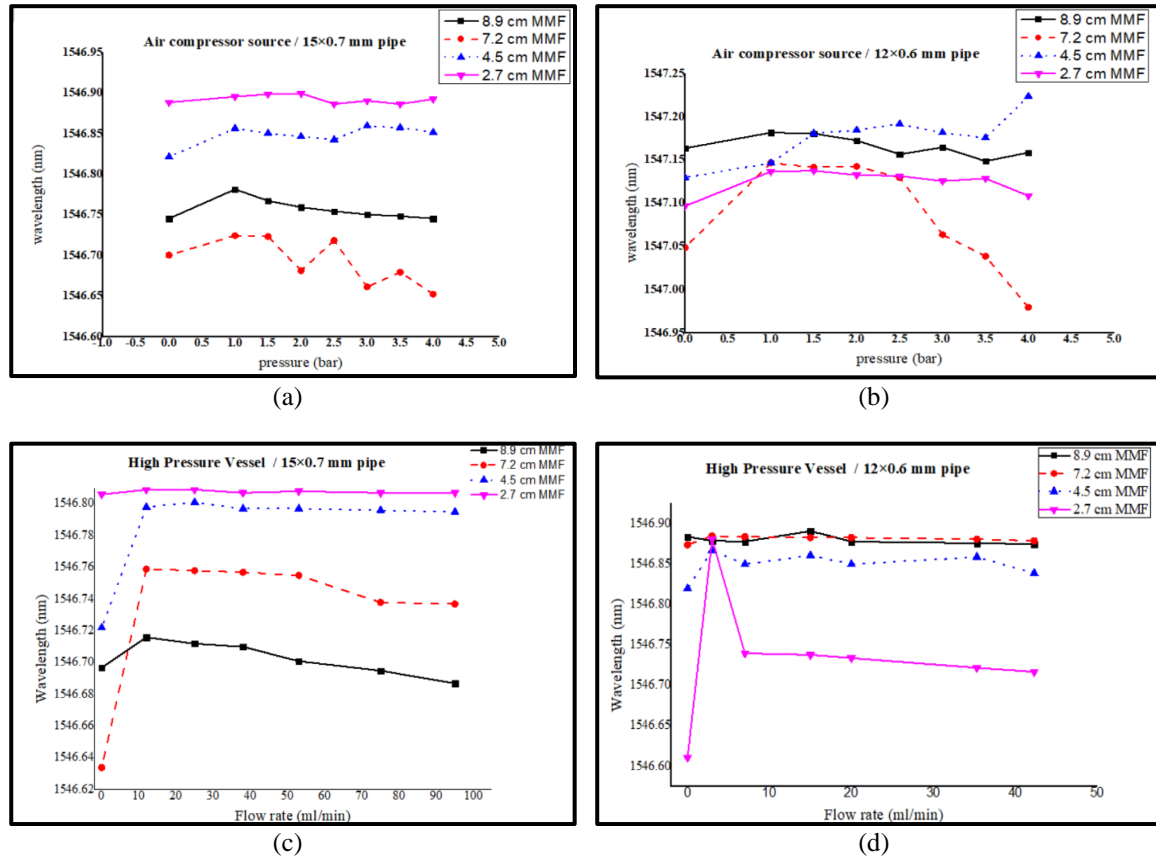| Sample in terms of MMF length	Compressor (pm/bar)		Cylinder (pm/bar)	
	15x.7	12x.6	15x.7	12x.6
8.9 cm	11.73	4.23	0.234	0.522
7.16cm	4.23	5.94	0.3771	0.5049
4.5 cm	5.84	20.93	0.3014	0.304
2.7 cm	4.69	7.79	0.17143	1.329

(a)

(b)

(c)

(d)

Figure 10. The experimental results of the wavelength shift under the effect of gas leakage (a), (b) stand for 15×0.7 mm and 12×0.6 mm pipe respectively provided with fixed flow and variable pressure out from air compressor and (c), (d) stand for 15×0.7 mm, and 12×0.6 mm pipe respectively provided with variable flow and variable pressure out from gas cylinder

The wavelength shift results are summarized in Figure 10 shows that the clad thickness size affects the position of the central wavelength transmitted by the interferometer around 0.2-0.3 nm. The existence of a leak induces a rapid redshift of about 50 pm/bar to the central wavelength of the applied laser source in almost all of the investigated cases. However, this shift was changed slightly into shorter wavelengths in most of the investigated cases, when the applied pressure of the leaked gas or its flow rate is changed. This turn into shorter wavelengths shift is around 10-40 pm/bar can be attributed to slight vibrations occurred by the gas flow rate at the sensing region of the interferometer which in turn modifies the phase of interfered signal and the center of the constructive interference. The wavelength shift Figures showed almost similar behavior related to size of the medical pipe regardless to the gas source as illustrated in Figure 10(a) and (b) of the 15×0.7 mm pipe size, we can see that the thicker clad and longer interferometer has shorter central wavelength while the shorter fiber and thinner clad has longer central wavelength and this relation is fixed for all applied pressures and flow rates. In contrast to the 12×0.6 mm pipe sample which shows less spacing between the curves of the used interferometer samples. In terms of sensitivity this work experiment showed that the 12x0.6 mm pipe size has higher sensitivity in range of 20.93 pm/bar in the case of 4.5 cm, 20 min etched sample of 89.7 µm clad size, this high sensitivity was obtained for low pressures in range of 1 to 4 bar. However, when higher pressure was applied on the same pipe by a gas cylinder then the 2 cm length of 69.6 µm clad size sample showed the higher

sensitivity. In contrast to the 15x0.7 mm pipe size, the highest sensitivity of both high and low-pressure gas were obtained by 7.16 cm, 10 min etched sample. From this result we can conclude that each different pipeline size requires different sensing. These results showed better recognizable and enhanced behavior than our previous work that used FBG only and obtained a sensitivity of 1 pm/bar for low pressure range 1-4 bars with more compact implementation capabilities [38]. Figure 10(c) and (d) shows that when both gas pressure and flow rate of the exposed leak are variable; then the central wavelength of each FP-MZI corresponding to its MMF clad thickness became closed to each other except the case of very thin clad 69 µm.

The obtained sensitivity of Table 3 can be compared to the Chen *et al*. [39] who used extrinsic fiber Fabry-Perot cavity and obtained 1.6 nm/MPa since MPa=10 bar then they obtained 160 pm/bar but for isolated in chamber sensing head, then this work result is considered a good result for intrinsic FP cavity without chamber. In terms of power losses along the interferometer, Figure 11 shows that output power ranged from 200-800 µW while the input power was equal to 1.3 mW that mean about 2-8 dB was the overall developed losses along with the whole investigated cases. The not etched fiber sample (MMF of 8.9 cm length) showed less sensitivity to environmental changes, almost best homogeneous response to the induced leak, and higher transmitted power as shown in Figure 11 in addition to better immunity to the high-pressure (10-100 bars) of the gas cylinder because it showed highest obtained power with lowest loss 2 dB. Moreover, the not etched fiber of 8.9 cm length showed higher output power than etched one as shown in Figure 11(b) and (c), and Figure 11(d). But the air compressor was used with larger pipe of 15×0.7 mm size, the obtained peak obtained power was the highest in the case of 20 min etched MMF and 4.5 cm sample length as illustrated in Figure 11(a).
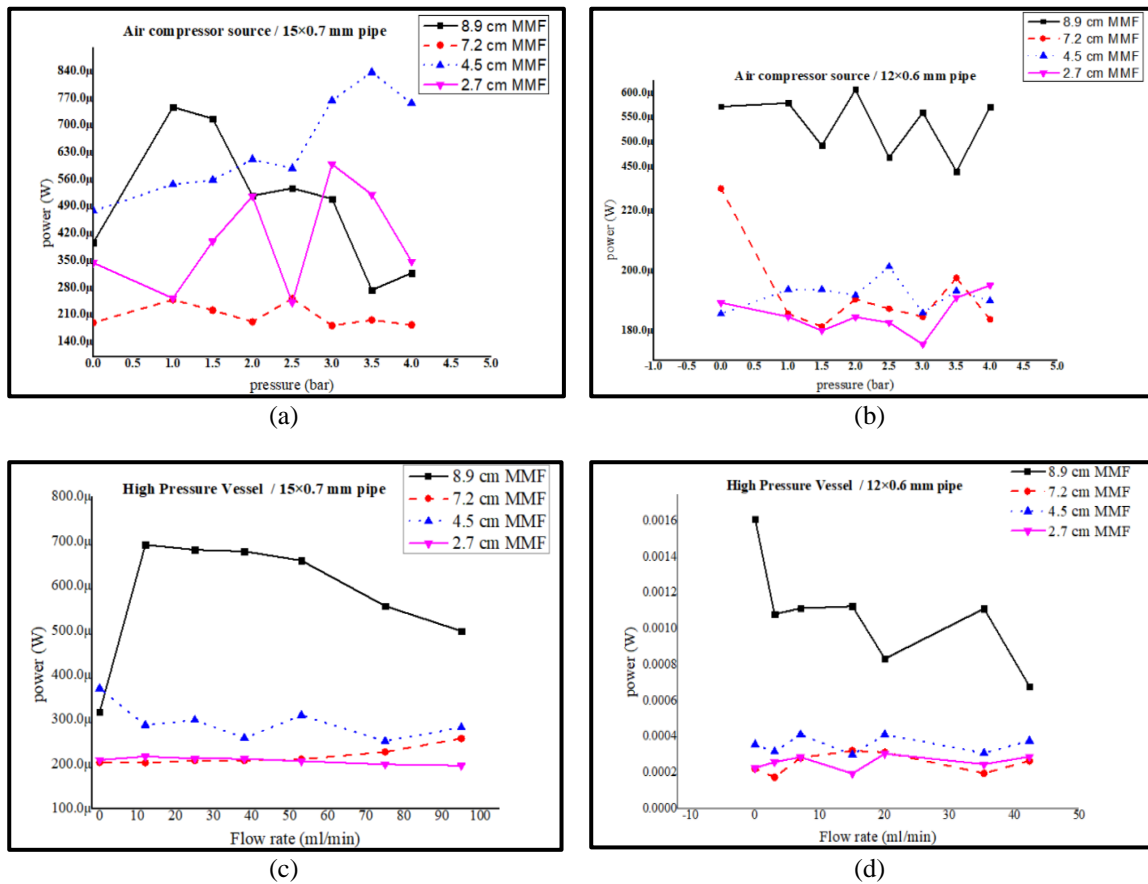

Figure 11. The power change under the effect of gas leaked from (a), (b) stand for 15×0.7 mm and 12×0.6 mm pipe respectively provided with fixed flow and variable pressure out from air compressor and (c), (d) stand for 15×0.7 mm, and 12×0.6 mm pipe respectively provided with variable flow and variable pressure out from gas cylinder

5.   CONCLUSION

A novel hybrid inline fiber interferometer structure that is based on hybrid interference between forward and backward waves of FBGs Fabry-Perot interferometer and arms of Mach-Zehnder interferometer generated by cascading of single and multi-modes fibers was investigated in this work. A Novel pipeline leakage detection of medical gases was investigated in this work using the proposed interferometer sensor for both cases of gas providing systems; fixed air compressor and portable gas vessel implemented according to BS slandered. The proposed interferometer was design according to analytical solution using MATLAB and tested using COMSOL software to insure interference at of the designed wavelength. The main conclusions that can be figured from this study; i) compact in size with few millimeters' sensor can be implemented with low loss power due the FBG-FP cavity behavior; ii) sensitivity in the range of 0.17-20.9 pm/bar was obtained from different samples investigated by this work proposed interferometer. This range of sensitivity is varied for different investigated samples of interferometer and pipe size; iii) each pipeline size has different behavior and required different etching period and clad size. Wider pipes required thicker clad while finer pipe showed better sensitivity with thinner clad; and vi) etching enhance sensitivity especially in the lower range of gas pressures but the longer etching period make the fiber more fragile and can't overcome with sever environment because many fractures and failures occurred with sample of 69.6 µm clad and 2.7 cm MMF length.

6.   RECOMMENDATION

Hybrid interferometer of this work can be investigated for distributed sensing network along the gases pipelines and connected in a network to control room for monitoring and protection of hospitals with smart algorithm of detection. Testing this interferometer for natural gas pipeline system experimentally and for biological blood measurements and applications.

REFERENCES

[1]   P. Stajanca, S. Chruscicki, T. Homann, S. Seifert, D. Schmidt, and A. Habib, "Detection of leak-induced pipeline vibrations using fiber—Optic distributed acoustic sensing," *Sensors (Switzerland)*, vol. 18, no. 9, p. 2841, Aug. 2018, doi: 10.3390/s18092841.
[2]   Q. Wu *et al.*, "Singlemode-multimode-singlemode fiber structures for sensing applications-a review," *IEEE Sensors Journal*, vol. 21, no. 11, pp. 12734–12751, Jun. 2021, doi: 10.1109/JSEN.2020.3039912.
[3]   A. Mishra, S. H. Al Gabani, and A. J. Al Hosany, "Pipeline leakage detection using fiber optics distributed temperature sensing DTS," in *Society of Petroleum Engineers - SPE Abu Dhabi International Petroleum Exhibition and Conference 2017*, Nov. 2017, vol. 2017-January, doi: 10.2118/188407-ms.
[4]   Q. Wang, L. Han, X. Fan, and J. Zhu, "Distributed fiber optic vibration sensor based on polarization fading model for gas pipeline leakage testing experiment," *Journal of Low Frequency Noise Vibration and Active Control*, vol. 37, no. 3, pp. 468–476, Sep. 2017, doi: 10.1177/1461348417725949.
[5]   Y. Huang, Q. Wang, L. Shi, and Q. Yang, "Underwater gas pipeline leakage source localization by distributed fiber-optic sensing based on particle swarm optimization tuning of the support vector machine," *Applied Optics*, vol. 55, no. 2, p. 242, Jan. 2016, doi: 10.1364/ao.55.000242.
[6]   M. Nikles, "Long-distance fiber optic sensing solutions for pipeline leakage, intrusion, and ground movement detection," in *Fiber Optic Sensors and Applications VI*, May 2009, vol. 7316, p. 731602, doi: 10.1117/12.818021.
[7]   A. Arifin, Y. Aryani, M. Yunus, and D. Tahir, "Electric current and magnetic field sensor based on plastic optical fiber and magnetic fluid," *Journal of Physics: Conference Series*, vol. 1120, no. 1, p. 012078, Nov. 2018, doi: 10.1088/1742-6596/1120/1/012078.
[8]   M. Shakeri *et al.*, "An overview of the building energy management system considering the demand response programs, smart strategies and smart grid," *Energies*, vol. 13, no. 13, p. 3299, Jun. 2020, doi: 10.3390/en13133299.
[9]   F. R. Bassan *et al.*, "Power-over-fiber LPIT for voltage and current measurements in the medium voltage distribution networks," *Sensors (Switzerland)*, vol. 21, no. 2, pp. 1–24, Jan. 2021, doi: 10.3390/s21020547.
[10] M. M. Gizeev, P. E. Denisenko, K. A. Lipatnikov, A. A. Kuznetsov, and E. P. Denisenko, "Fiber optic sensor systems for non-destructive monitoring of 'smart buildings,'" *Journal of Physics: Conference Series*, vol. 1327, no. 1, p. 012025, Oct. 2019, doi: 10.1088/1742-6596/1327/1/012025.
[11] S. P. Raj, N. S. Kavitha, S. S. Rachel, and P. Suganthi, "Smart hospitals E-medico management system," *International Journal of Recent Technology and Engineering*, vol. 8, no. 3, pp. 4651–4655, Sep. 2019, doi: 10.35940/ijrte.C6841.098319.
[12] N. M. Hussien, Y. M. Mohialden, N. T. Ahmed, M. A. Mohammed, and T. Sutikno, "A smart gas leakage monitoring system for use in hospitals," *Indonesian Journal of Electrical Engineering and Computer Science*, vol. 19, no. 2, pp. 1048–1054, Aug. 2020, doi: 10.11591/ijeecs.v19.i2.pp1048-1054.
[13] G. P. Agrawal, *Applications of Nonlinear Fiber Optics*. Elsevier, 2008, doi: 10.1016/B978-0-12-374302-2.X5001-3.
[14] D. J. Webb, *Polymer fiber bragg grating sensors and their applications*. CRC Press, 2017, doi: 10.1201/b18074.
[15] N. F. Noori and T. S. Mansour, "Design and construction of tunable band pass filter using hybrid FPMZI," *Design Engineering*, pp. 6959–6972, 2021.
[16] B. H. Mutar and T. S. Mansour, "Design of tunable optical band pass filter based on in-Line PM-Mach Zehnder interferometer," *Iraqi Journal of Laser*, vol. 20, no. 1, pp. 6–12, 2021.
[17] X. Lei, X. Dong, C. Lu, T. Sun, and K. T. V. Grattan, "Underwater pressure and temperature sensor based on a special dual-mode optical fiber," *IEEE Access*, vol. 8, pp. 146463–146471, 2020, doi: 10.1109/ACCESS.2020.3015195.
[18] M. M. Hasan, H. J. Taher, and S. A. Mohammed, "Highly sensitive fiber-optic temperature sensor based on tapered no-core fiber for biomedical and biomechanical applications," *Periodicals of Engineering and Natural Sciences (PEN)*, vol. 9, no. 2, p. 762, Apr. 2021, doi: 10.21533/pen.v9i2.1892.

[19] A. Miliou, "In-fiber interferometric-based sensors: overview and recent advances," *Photonics*, vol. 8, no. 7, p. 265, Jul. 2021, doi: 10.3390/photonics8070265.

[20] N. Hamza, "Enhanced refractive index sensor based on etched coreless fiber," *Authorea Preprints*, no. Mmi, 2020.

[21] S. H. Patil, A. Saha, and M. D. Barma, "Performance analysis of cladding etched fiber bragg grating based refractive index sensor," in *2018 2nd International Conference on Electronics, Materials Engineering & Nano-Technology (IEMENTech)*, May 2018, pp. 1–3, doi: 10.1109/IEMENTECH.2018.8465251.

[22] C. E. Lee, W. N. Gibler, R. A. Atkins, and H. F. Taylor, "In-line fiber Fabry-Perot interferometer with high-reflectance internal mirrors," *Journal of Lightwave Technology*, vol. 10, no. 10, pp. 1376–1379, 1992, doi: 10.1109/50.166779.

[23] H. Cheng, S. Wu, Q. Wang, S. Wang, and P. Lu, "In-line hybrid fiber sensor for curvature and temperature measurement," *IEEE Photonics Journal*, vol. 11, no. 6, pp. 1–11, Dec. 2019, doi: 10.1109/JPHOT.2019.2944988.

[24] J. Wang *et al.*, "Temperature insensitive fiber Fabry-Perot/Mach-Zehnder hybrid interferometer based on photonic crystal fiber for transverse load and refractive index measurement," *Optical Fiber Technology*, vol. 56, p. 102163, May 2020, doi: 10.1016/j.yofte.2020.102163.

[25] B. Xu, Y. Yang, Z. Jia, and D. N. Wang, "Hybrid Fabry-Perot interferometer for simultaneous liquid refractive index and temperature measurement," *Optics Express*, vol. 25, no. 13, p. 14483, Jun. 2017, doi: 10.1364/oe.25.014483.

[26] H. Sun *et al.*, "A hybrid fiber interferometer for simultaneous refractive index and temperature measurements based on Fabry–Perot/Michelson interference," *IEEE Sensors Journal*, vol. 13, no. 5, pp. 2039–2044, May 2013, doi: 10.1109/JSEN.2013.2246862.

[27] M. Sun, Y. Jin, and X. Dong, "All-fiber Mach–Zehnder interferometer for liquid level measurement," *IEEE Sensors Journal*, vol. 15, no. 7, pp. 3984–3988, Jul. 2015, doi: 10.1109/JSEN.2015.2406872.

[28] X.-P. Luo *et al.*, "A novel Mach–Zehnder interferometer based on hybrid liquid crystal–photonic crystal fiber," *Chinese Physics Letters*, vol. 34, no. 12, p. 124203, Dec. 2017, doi: 10.1088/0256-307X/34/12/124203.

[29] Y. Wang, Y. Zhou, Z. Liu, D. Chen, C. Lu, and H.-Y. Tam, "Sensitive Mach–Zehnder interferometric sensor based on a grapefruit microstructured fiber by lateral offset splicing," *Optics Express*, vol. 28, no. 18, p. 26564, Aug. 2020, doi: 10.1364/OE.402584.

[30] X. Fu *et al.*, "A few mode fiber temperature sensor filled with PDMS based on Vernier effect," *IEEE Photonics Journal*, vol. 13, no. 5, pp. 1–5, Oct. 2021, doi: 10.1109/JPHOT.2021.3112125.

[31] R. E. Izzaty, B. Astuti, and N. Cholimah, *Optical fiber telecommunications V A components and subsystem*. Academic Press, 1967.

[32] B. A. Taha *et al.*, "Comprehensive review tapered optical fiber configurations for sensing application: trend and challenges," *Biosensors*, vol. 11, no. 8, p. 253, Jul. 2021, doi: 10.3390/bios11080253.

[33] L. B. Soldano and E. C. M. Pennings, "Optical multi-mode interference devices based on self-imaging: principles and applications," *Journal of Lightwave Technology*, vol. 13, no. 4, pp. 615–627, Apr. 1995, doi: 10.1109/50.372474.

[34] S. Novais, M. Ferreira, and J. Pinto, "Relative humidity fiber sensor based on multimode interferometer coated with agarose-gel," *Coatings*, vol. 8, no. 12, p. 453, Dec. 2018, doi: 10.3390/coatings8120453.

[35] H. Alsweefe, S. K. Al-Hayali, and A. Al-Janabi, "Efficient humidity sensor based on an etched no-core fiber coated with copper oxide nanoparticles," *Journal of Nanophotonics*, vol. 12, no. 04, p. 1, Dec. 2018, doi: 10.1117/1.JNP.12.046018.

[36] J. R. Guzmán-Sepúlveda, R. Guzmán-Cabrera, and A. A. Castillo-Guzmán, "Optical sensing using fiber-optic multimode interference devices: a review of nonconventional sensing schemes," *Sensors*, vol. 21, no. 5, Mar. 2021, doi: 10.3390/s21051862.

[37] B. H. Mutar, N. F. Noori, Y. I. Hammadi, and T. S. Mansour, "In-line fiber tunable pulse compressor using PM-Mach Zehnder interferometer," *Journal of Mechanical Engineering Research and Developments*, vol. 44, no. 5, pp. 287–297, 2021.

[38] F. M. Abdulhussein, "Dual measurements of pressure and temperature with fiber bragg grating dual measurements of pressure and temperature with fiber bragg grating sensor," *Al-Khwarizmi Engineering Journal*, 2019.

[39] J. Chen *et al.*, "Influence of temperature on all-silica Fabry-Pérot pressure sensor," *IEEE Photonics Journal*, vol. 13, no. 3, pp. 1–9, Jun. 2021, doi: 10.1109/JPHOT.2021.3083808.

BIOGRAPHIES OF AUTHORS

Nada F. Noori 🆔 Ⓖ SC ⮂ Received the B.Eng. degree in Laser and optoelectronics engineering from Al-Nahrain University, Baghdad, in 2008 and the M.S. also in Laser and optoelectronics engineering from Al-Nahrain University, Baghdad, in 2014. Currently Ph.D. student in Institute of laser for post graduate studies at university of Baghdad, and employee at the national center for engineering consultancy, department of electrical designs, Iraq. Research interests include optical communications, optical fibers, optical sensor, laser systems, optical networks, interferometers. She can be contacted at email: nada.fares1101a@ilps.uobaghdad.edu.iq.

Tahreer S. Mansour 🆔 Ⓖ SC ⮂ Holds a Ph.D. in electronics and communication engineering from University of Baghdad, Iraq. She is currently a professor assistant and Head of the department of industrial and engineering applications of the Institute of laser for post graduate studies at the University of Baghdad. She was the head of the photonic applications department at the same institute of university of Baghdad. She has authored or coauthored around 56 publication refereed journal and conference papers, her research interests include the applications of optical communications, optical fibers, plasmonic, biomedical applications. She can be contacted at email: tahreer@ilps.uobaghdad.edu.iq.